Appl. Math. Mech. -Engl. Ed., **42**(4), 593–606 (2021)

APPLIED MATHEMATICS AND MECHANICS (ENGLISH EDITION)

https://doi.org/10.1007/s10483-021-2727-8

Electro-magneto-hydrodynamic flow of couple stress nanofluids in micro-peristaltic channel with slip and convective conditions*

K. RAMESH[1], M. G. REDDY[2], B. SOUAYEH[3,4,†]

1. Department of Mathematics, Symbiosis Institute of Technology, Symbiosis International (Deemed University), Pune 412115, India;
2. Department of Mathematics, Acharya Nagarjuna University, Ongole Campus, Ongole 523001, India;
3. Department of Physics, College of Science, King Faisal University, Al-Ahsa 31982, Saudi Arabia;
4. Laboratory of Fluid Mechanics, Physics Department, Faculty of Sciences of Tunis, University of Tunis El Manar, Tunis 2092, Tunisia

(Received Oct. 11, 2020 / Revised Feb. 5, 2021)

Abstract This study explores the effects of electro-magneto-hydrodynamics, Hall currents, and convective and slip boundary conditions on the peristaltic propulsion of nanofluids (considered as couple stress nanofluids) through porous symmetric micro-channels. The phenomena of energy and mass transfer are considered under thermal radiation and heat source/sink. The governing equations are modeled and non-dimensionalized under appropriate dimensionless quantities. The resulting system is solved numerically with MATHEMATICA (with an in-built function, namely the Runge-Kutta scheme). Graphical results are presented for various fluid flow quantities, such as the velocity, the nanoparticle temperature, the nanoparticle concentration, the skin friction, the nanoparticle heat transfer coefficient, the nanoparticle concentration coefficient, and the trapping phenomena. The results indicate that the nanoparticle heat transfer coefficient is enhanced for the larger values of thermophoresis parameters. Furthermore, an intriguing phenomenon is observed in trapping: the trapped bolus is expanded with an increase in the Hartmann number. However, the bolus size decreases with the increasing values of both the Darcy number and the electroosmotic parameter.

Key words peristalsis, magnetohydrodynamics (MHD), nanofluid, Hall current, porous medium, thermal radiation

Chinese Library Classification O361
2010 Mathematics Subject Classification 76Z05, 76W05, 76A05

* Citation: RAMESH, K., REDDY, M. G., and SOUAYEH, B. Electro-magneto-hydrodynamic flow of couple stress nanofluids in micro-peristaltic channel with slip and convective conditions. *Applied Mathematics and Mechanics* (*English Edition*), **42**(4), 593–606 (2021) https://doi.org/10.1007/s10483-021-2727-8

† Corresponding author, E-mail: bsouayeh@kfu.edu.sa

1 Introduction

Peristalsis is a systematic mechanism for carrying and moving fluids. This mechanism is based on the relaxation and contraction of waves in the channel containing the fluid. This phenomenon is typically encountered in physiological systems through mechanical contraction of extensible vessel walls. It is also encountered in industry and physiology, including transport of food through the esophagus[1], embryonic lung morphogenesis[2], transport of chyme in the intestine[3], propulsion of bile in the bile duct, motion of corrosive fluids, and transport of sanitary fluids. Numerous experimental investigations have been performed on the peristaltic motion[4–5]. However, a greater focus is still needed on this phenomenon from the mathematical and computational perspectives. In previous studies, many parameters were considered, such as the types of synchronous vessel oscillation, various physiological fluids, and wall properties. Moreover, recent studies can be found in the references[6–14] about the direction of peristaltic flows. Earlier, Hlew et al.[15] started working on some physiological transport phenomena by studying fluid propulsion by peristalsis of the small intestine. For this purpose, a mathematical model was developed for a viscous fluid in a tube geometry. Tripathi[16] developed a model to analyze the peristaltic chyme (viscoelastic fluid) flow in the small intestine using a cylindrical tube. The peristaltic propulsion of a rigid spherical bolus in a contractile membrane was numerically performed by Bertuzzi et al.[17]. Moradi et al.[18] numerically investigated the peristaltic motion of Newtonian incompressible liquids in annular geometries. The surface waves were superposed with the flow in the annulus by forming axisymmetric waves to achieve the peristaltic effect. Tsui[19] used a multi-dimensional calculation method to simulate peristaltic micro-pump flows. Kumar and Naidu[20] employed a nonlinear streamline quadrature up-winding non-iterative method to solve a two-dimensional (2D) peristaltic flow. A numerical simulation intended to model a soft-acting peristaltic pump was presented by Natarajan and Mokhtarzadeh[21]; this model is useful in the design of blood pumping systems. Radhakrishnamacharya and Srinivasulu[22] analyzed the peristaltic propulsion of viscous liquids in a 2D uniform channel. The hydrodynamic stability of peristaltic waves in a deformable conduit was presented by Chu[23]. The electrostatically peristaltic micro-pump design and simulation were investigated by Lin et al.[24]. Several investigations on peristaltic pumping simulation, analysis, and design were conducted[25–27]. Afifi and Gad[28] employed a mathematical model based on a viscous incompressible fluid flow between infinite parallel walls to analyze the peristaltic motion with a porous medium.

It is normally observed that nanofluids have higher thermal conductivities. In view of this, traditional nanoliquids with base liquids, such as water, oil, and ethylene glycol mixtures have been used to enhance the heat transfer. Metals (e.g., iron, copper, and zinc) typically have higher thermal conductivities than pure liquids. The mixing of nanoparticles into the base liquids generates better transport and thermophysical properties for the nanoliquids. Nanofluids significantly increase the capability of heat transfer owing to their amplified thermal diffusivity and thermal conductivity[29]. Several investigations examined the exclusive features of nanofluids under different flow configurations owing to their useful utility in many engineering and industrial applications. Few studies[30–40] for various situations can be found in the field of nanofluids. The peristaltic motion of nanoliquids is vital in current medication conveyance frameworks in which attractive transitions are utilized to manage the nanoparticles in the circulation system to the tumor site. Among many challenges, the peristaltic propulsion of nanoliquids is now focused on certain endeavors. For example, Hayat et al.[41] investigated the slip consequences on the peristaltic motion of nanofluids using Buongiorno's model (BM). The same methodology was used to investigate the peristaltic motion of nanoliquids in the studies conducted by Abbasi et al.[42] and Shehzad et al.[43]. The aforementioned studies paid less attention to the direction of magnetic nanoparticles. A nanofluid flow under the influence of magnetohydrodynamics (MHD) plays a crucial role in industrial manufacturing and biomedical

processes. Noreen et al.[44] discussed the propulsion of MHD nanofluids in a peristaltic channel. Hayat et al.[45] used Carreau nanofluids to discuss the fluid flow in peristalsis under radial MHD effects. Hayat et al.[46] discussed the effects of MHD, slip, and Joule heating on the propulsion of hyperbolic tangent nanomaterials. Shehzad et al.[47] investigated the effects of MHD, thermophoresis, and Joule heating on the peristaltic motion of nanoliquids. The effects of MHD, Joule heating, and wall characteristics on the peristaltic flow of nanoliquids were studied by Hayat et al.[48].

Among the previous studies mentioned above, there have been no studies addressing the simultaneous influences of magnetic and electrical fields of couple stress nanofluids in micro-peristaltic channels under convective and slip boundary conditions with the Runge-Kutta integration scheme. To fill this gap, we propose a new model to discuss the propulsion of couple stress nanofluids through peristaltic micro-channels. The effects of the electrical field, magnetic field, Hall currents, porous medium, thermal radiation, and slip and convective boundary conditions have been considered. The consequences of pertinent factors on the characteristics of flow, such as nanoparticle concentration and heat and mass transfer coefficients, are presented.

2 Mathematical modeling

2.1 Problem formulation

We analyze the propulsion of couple stress nanofluids through a peristaltic micro-channel of the width $2d$. The effects of the electric field, magnetic field, Hall currents, thermal radiation, heat source/sink, and convective and slip boundary conditions are considered. The Cartesian coordinate system is assumed for the proposed analysis, with the X-axis parallel to the wave propagation and the Y-axis transverse to the flow situation. The uniform magnetic field B_0 is considered to be in the opposite direction of the flow. The complete geometry of the micro-peristaltic channel is shown in Fig. 1.

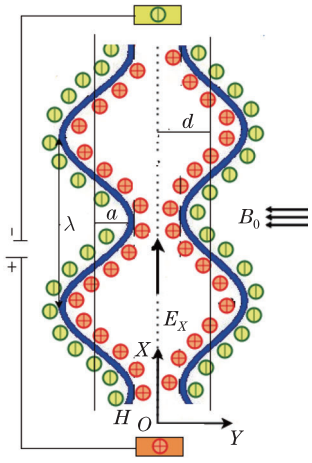

Fig. 1 Geometry of symmetric peristaltic channel (color online)

The walls of the aforementioned problem can be expressed as[49]

$$H(X,t) = \pm\left(d - a\cos^2\left(\frac{\pi}{\lambda}(X - ct)\right)\right). \tag{1}$$

Here, d, a, λ, c, and t are the channel's half-width, channel's wave amplitude, wavelength, wave speed, and time, respectively. The governing equations can be expressed for a couple stress nanofluid flow as follows[49–51]:

$$\frac{\partial U}{\partial X} + \frac{\partial V}{\partial Y} = 0, \tag{2}$$

$$\rho_{\mathrm{f}}\Big(\frac{\partial U}{\partial t}+U\frac{\partial U}{\partial X}+V\frac{\partial U}{\partial Y}\Big)=-\frac{\partial P}{\partial X}+\mu_{\mathrm{f}}\Big(\frac{\partial^2 U}{\partial X^2}+\frac{\partial^2 U}{\partial Y^2}\Big)-\eta\Big(\frac{\partial^4 U}{\partial X^4}+2\frac{\partial^4 U}{\partial X^2\partial Y^2}+\frac{\partial^4 U}{\partial Y^4}\Big)$$
$$-\frac{\sigma_{\mathrm{f}}B_0^2U}{1+m^2}-\frac{\mu_{\mathrm{f}}\phi_1 U}{k_0}+\rho_{\mathrm{e}}E_X+(1-C_0)\rho_{\mathrm{f}}g\beta_{\mathrm{t}}(T-T_0)$$
$$-(\rho_{\mathrm{p}}-\rho_{\mathrm{f}})g\beta_{\mathrm{c}}(C-C_0), \tag{3}$$

$$\rho_{\mathrm{f}}\Big(\frac{\partial V}{\partial t}+U\frac{\partial V}{\partial X}+V\frac{\partial V}{\partial Y}\Big)=-\frac{\partial P}{\partial Y}+\mu_{\mathrm{f}}\Big(\frac{\partial^2 V}{\partial X^2}+\frac{\partial^2 V}{\partial Y^2}\Big)-\eta\Big(\frac{\partial^4 V}{\partial X^4}+2\frac{\partial^4 V}{\partial X^2\partial Y^2}+\frac{\partial^4 V}{\partial Y^4}\Big)$$
$$-\frac{\mu_{\mathrm{f}}\phi_1 V}{k_0}, \tag{4}$$

$$(\rho c')_{\mathrm{f}}\Big(\frac{\partial T}{\partial t}+U\frac{\partial T}{\partial X}+V\frac{\partial T}{\partial Y}\Big)=\alpha_1\Big(\frac{\partial^2 T}{\partial X^2}+\frac{\partial^2 T}{\partial Y^2}\Big)-\Big(\frac{\partial q_{\mathrm{r}}}{\partial X}+\frac{\partial q_{\mathrm{r}}}{\partial Y}\Big)$$
$$+(\rho c')_{\mathrm{p}}\bigg(D_{\mathrm{B}}\Big(\frac{\partial C}{\partial X}\frac{\partial T}{\partial X}+\frac{\partial C}{\partial Y}\frac{\partial T}{\partial Y}\Big)$$
$$+\frac{D_{\mathrm{T}}}{T_{\mathrm{m}}}\Big(\Big(\frac{\partial T}{\partial X}\Big)^2+\Big(\frac{\partial T}{\partial Y}\Big)^2\Big)\bigg)+Q_0(T-T_0), \tag{5}$$

$$\Big(\frac{\partial C}{\partial t}+U\frac{\partial C}{\partial X}+V\frac{\partial C}{\partial Y}\Big)=D_{\mathrm{B}}\Big(\frac{\partial^2 C}{\partial X^2}+\frac{\partial^2 C}{\partial Y^2}\Big)+\frac{D_{\mathrm{T}}}{T_{\mathrm{m}}}\Big(\Big(\frac{\partial T}{\partial X}\Big)^2+\Big(\frac{\partial T}{\partial Y}\Big)^2\Big), \tag{6}$$

where the parameters U and V are the velocities in the flow and transverse directions, respectively. ρ_{f}, ρ_{e}, and ρ_{p} represent the density of fluids, the electrical charge density, and the density of nanoparticles, respectively. P is the dimensional fixed frame pressure. μ_{f} is the effective dynamic viscosity of nanofluids, and η is the dimensional couple stress fluid parameter. σ_{f} and m denote the effective electric conductivity and the Hall current parameter, respectively. ϕ_1 is the porosity of the medium, and k_0 is the permeability. E_X is the electric field. C_0 and C are the ambient nanoparticle concentration and the dimensional nanoparticle concentration, respectively, and g is the gravitational acceleration due to the gravity. β_{t} and β_{c} are the effective thermal expansion coefficient of nanoliquid and the expansion coefficient with concentration, respectively. T and T_0 are the dimensional temperature and the ambient temperature, respectively. c'_{f} and c'_{p} are the heat capacitances of fluids and nanoparticles, respectively. α_1 is the thermal conductivity of nanofluids, and q_{r} is the radiative heat flux. D_{B} and D_{T} are the Brownian diffusion coefficient and the thermophoretic diffusion coefficient, respectively. T_{m} is the mean temperature, and Q_0 is the volumetric rate of heat source. Equation (5) can be reduced with the help of the Rosseland approximation, which is given by $q_{\mathrm{r}}=-\frac{4\sigma^*}{3\alpha^*}\frac{\partial T^4}{\partial Y}$. The difference in temperature may be expanded in the form of Taylor's series such as T^4 about T_0, and after neglecting the higher terms, we obtain $T^4\cong 4T_0^3T-3T_0^4$, where σ^* and α^* represent the Stefan-Boltzmann constant and the mean absorption coefficient of nanofluids, respectively.

2.2 Electro-hydrodynamics

Poisson's equation of the electric potential Φ can be expressed as

$$\frac{\partial^2\Phi}{\partial X^2}+\frac{\partial^2\Phi}{\partial Y^2}=-\frac{\rho_{\mathrm{e}}}{\varepsilon_{\mathrm{ef}}}, \tag{7}$$

where ρ_{e} and $\varepsilon_{\mathrm{ef}}$ are the electrolyte net charge density in the presence of an electric double layer and the dielectric constant, respectively.

The electric charge density is given by

$$\rho_{\mathrm{e}}=-2n_0ez\sinh\Big(\frac{ez\Phi}{K_{\mathrm{B}}T_{\mathrm{e}}}\Big), \tag{8}$$

where n_0, e, z, K_{B}, and T_{e} represent the bulk concentration, the electric charge, the charge balance, the Boltzmann constant, and the absolute temperature, respectively.

With the help of Debye-Hückel linearization, Eq. (7) is reduced to

$$\frac{\partial^2\Phi}{\partial X^2}+\frac{\partial^2\Phi}{\partial Y^2}=\frac{2n_0e^2z^2}{\varepsilon_{\rm ef}K_{\rm B}T_{\rm e}}\Phi. \tag{9}$$

2.3 Wave frame transformations and scaling of governing equations

The transformations of fixed and wave frame of references can be introduced as follows:

$$x=X-ct,\quad y=Y,\quad u=U-c,\quad v=V,\quad p=P,\quad \overline{T}=T,\quad \overline{C}=C. \tag{10}$$

The scaling parameters for the current governing equations can be expressed as

$$\begin{cases}
\overline{x}=\dfrac{x}{\lambda},\quad \overline{y}=\dfrac{y}{d},\quad \overline{u}=\dfrac{u}{c},\quad \overline{v}=\dfrac{v}{c\delta},\quad \delta=\dfrac{d}{\lambda},\quad \overline{p}=\dfrac{d^2p}{\lambda\mu_{\rm f}c},\quad \theta=\dfrac{\overline{T}-T_0}{T_0},\\
\sigma=\dfrac{\overline{C}-C_0}{C_0},\quad a^2=\dfrac{\eta}{\mu_{\rm f}d^2},\quad Re=\dfrac{\rho_{\rm f}cd}{\mu_{\rm f}},\quad M=\sqrt{\dfrac{\sigma_{\rm f}}{\mu_{\rm f}}}B_0d,\quad D_{\rm a}=\dfrac{k_0}{\phi_1d^2},\\
Gr_{\rm t}=\dfrac{(1-C_0)d^2\rho_{\rm f}g\beta_{\rm t}T_0}{\mu_{\rm f}c},\quad Gr_{\rm c}=\dfrac{(\rho_{\rm f}-\rho_{\rm p})d^2g\beta_{\rm c}C_0}{\mu_{\rm f}c},\quad k=dez\sqrt{\dfrac{2n_0}{\varepsilon_{\rm ef}K_{\rm B}T_{\rm e}}},\quad \overline{\Phi}=\dfrac{\Phi}{\xi},\\
U_{\rm hs}=-\dfrac{\varepsilon_{\rm ef}\xi E_X}{\mu_{\rm f}c},\quad N_{\rm b}=\dfrac{\rho_{\rm f}(\rho c')_{\rm p}D_{\rm B}C_0}{\mu_{\rm f}(\rho c')_{\rm f}},\quad N_{\rm t}=\dfrac{\rho_{\rm f}(\rho c')_{\rm p}D_{\rm T}T_0}{\mu_{\rm f}(\rho c')_{\rm f}T_{\rm m}},\quad R_{\rm n}=\dfrac{16\sigma^*T_0^3}{3\alpha^*\mu_{\rm f}c'_{\rm f}},\\
Pr=\dfrac{\mu_{\rm f}c'_{\rm f}}{\alpha_1},\quad \gamma=\dfrac{Q_0d^2}{\mu_{\rm f}c'_{\rm f}}.
\end{cases} \tag{11}$$

Under the above wave transformations (see Eq. (10)), scaling parameters (see Eq. (11)), and the assumptions of long wavelength and lubrication, Eqs. (3)–(6) and Eq. (9) (after dropping the bars) are reduced to

$$\frac{\partial p}{\partial x}=\frac{\partial}{\partial y}\Big(\frac{\partial u}{\partial y}-a^2\frac{\partial^3u}{\partial y^3}\Big)-\Big(\frac{M^2}{1+m^2}+\frac{1}{D_{\rm a}}\Big)(u+1)+k^2U_{\rm hs}\Phi+Gr_{\rm t}\theta+Gr_{\rm c}\sigma, \tag{12}$$

$$\frac{\partial p}{\partial y}=0, \tag{13}$$

$$\Big(\frac{1+R_{\rm n}Pr}{Pr}\Big)\frac{\partial^2\theta}{\partial y^2}+N_{\rm b}\Big(\frac{\partial\theta}{\partial y}\frac{\partial\sigma}{\partial y}\Big)+N_{\rm t}\Big(\frac{\partial\theta}{\partial y}\Big)^2+\gamma\theta=0, \tag{14}$$

$$\frac{\partial^2\sigma}{\partial y^2}+\frac{N_{\rm t}}{N_{\rm b}}\frac{\partial^2\theta}{\partial y^2}=0, \tag{15}$$

$$\frac{\partial^2\Phi}{\partial y^2}=k^2\Phi. \tag{16}$$

By introducing non-dimensional stream functions for both velocity components such as $u=\frac{\partial\psi}{\partial y}$ and $v=-\frac{\partial\psi}{\partial x}$ in Eqs. (12) and (13), we obtain

$$\frac{\partial^2}{\partial y^2}\Big(\frac{\partial^2\psi}{\partial y^2}-a^2\frac{\partial^4\psi}{\partial y^4}\Big)-\Big(\frac{M^2}{1+m^2}+\frac{1}{D_{\rm a}}\Big)\frac{\partial^2\psi}{\partial y^2}+k^2U_{\rm hs}\frac{\partial\Phi}{\partial y}+Gr_{\rm t}\frac{\partial\theta}{\partial y}+Gr_{\rm c}\frac{\partial\sigma}{\partial y}=0, \tag{17}$$

where a is the couple stress nanofluid parameter. M is the Hartmann number. $D_{\rm a}$ and k are the Darcy number and the electro-osmosis parameter, respectively. $U_{\rm hs}$ is the Helmholtz-Smoluchowski velocity. $Gr_{\rm t}$ and $Gr_{\rm c}$ are the thermal Grashof number and the concentration Grashof number, respectively. $R_{\rm n}$ is the radiation parameter, and Pr is the Prandtl number. $N_{\rm b}$ and $N_{\rm t}$ are the Brownian motion parameter and the thermophoresis parameter, respectively. γ is the heat generation parameter, and u is the non-dimensional velocity. p is the dimensionless pressure gradient. θ and σ are the dimensionless temperature and the non-dimensional nanoparticle concentration, respectively, and Φ is the dimensionless electric potential.

2.4 Boundary conditions and volumetric flow rate

In the wave frame, the corresponding non-dimensional boundary conditions are

$$\begin{cases} \psi = \dfrac{F}{2}, \quad \dfrac{\partial \psi}{\partial y} + \alpha\Big(\dfrac{\partial^2 \psi}{\partial y^2} - a^2 \dfrac{\partial^4 \psi}{\partial y^4}\Big) = -1, \quad \dfrac{\partial^3 \psi}{\partial y^3} = 0, \quad \dfrac{\partial \theta}{\partial y} + B_{\mathrm{h}}\theta = 0, \\ \dfrac{\partial \sigma}{\partial y} + B_{\mathrm{m}}\sigma = 0 \quad \text{at} \quad y = h, \end{cases} \tag{18}$$

$$\begin{cases} \psi = -\dfrac{F}{2}, \quad \dfrac{\partial \psi}{\partial y} - \alpha\Big(\dfrac{\partial^2 \psi}{\partial y^2} - a^2 \dfrac{\partial^4 \psi}{\partial y^4}\Big) = -1, \quad \dfrac{\partial^3 \psi}{\partial y^3} = 0, \quad \dfrac{\partial \theta}{\partial y} - B_{\mathrm{h}}\theta = 0, \\ \dfrac{\partial \sigma}{\partial y} - B_{\mathrm{m}}\sigma = 0 \quad \text{at} \quad y = -h, \end{cases} \tag{19}$$

where F, α, B_{h}, and B_{m} are the instantaneous average volume rate, the dimensionless slip parameter, the thermal Biot number, and the concentration Biot number, respectively. The dimensionless walls are defined as $y = \pm(1 - \phi\cos^2(\pi x))$. The flow rate is defined between the fixed and wave frames of reference as follows:

$$Q = F + 1 - h - \frac{\phi}{2}, \tag{20}$$

where $F = \int_0^h u\mathrm{d}y$, Q and F are the non-dimensional flux rates in the fixed and wave frames, respectively, and ϕ is the wave amplitude ratio.

2.5 Physical parameters of engineering interest

The expressions for the non-dimensional skin friction, the nanoparticle heat transfer coefficient, and the nanoparticle concentration coefficient at the walls are given by

$$C_{\mathrm{f}} = \frac{\partial h}{\partial x}\Big(\frac{\partial u}{\partial y} - a^2 \frac{\partial^3 u}{\partial y^3}\Big)_{y=h}, \tag{21}$$

$$Nu = \frac{\partial h}{\partial x}\Big(\frac{\partial \theta}{\partial y}\Big)_{y=h}, \tag{22}$$

$$Sh = \frac{\partial h}{\partial x}\Big(\frac{\partial \sigma}{\partial y}\Big)_{y=h}. \tag{23}$$

3 Results and discussion

The governing equations (12)–(17) are solved using a numerical procedure with the help of NDSolve MATHEMATIC under suitable boundary conditions. This section is focused on the influence of various quantities on the axial velocity u, the nanoparticle temperature θ, the nanoparticle concentration σ, the skin-friction coefficient C_{f}, the nanoparticle heat transfer coefficient Nu, the nanoparticle concentration coefficient Sh, and the trapping phenomenon.

Figures 2–6 show the effects of the Hartmann number M, the Darcy number D_{a}, the couple stress parameter a, the electro-osmotic parameter k, and the velocity slip parameter α on the velocity distributions. The velocity decreases near the middle of the channel, and the trend is reversed near the walls with an increase in the Hartmann number. This reduction is caused by the Lorentz force, which is a resistive force that leads to a reduction in the velocity at the centre of the channel (see Fig. 2). Figures 3–4 illustrate the influences of the Darcy number and the couple stress parameter on the velocity profiles. It is clear that, the velocity decreases near the channel walls and is enhanced in the center part of the channel. A higher Darcy number provides a nearly clear medium, whereas a lower Darcy number provides a porous medium with more voids. For this reason, higher velocities are observed near the center of the channel. Moreover, note from Fig. 4 that higher velocities are observed for the couple stress nanofluid than for the viscous nanofluid. Figure 5 shows that the velocity increases near the channel walls, and decreases near the center of the channel with an increase in the electro-osmotic parameter. This is due to the electrical double layer (EDL) effect, and the EDL acts as a resistive

agent for the fluid flows. For this reason, the velocity decreases in the middle of the channel. Figure 6 depicts the effect of different slip parameters on the velocity. It is shown that the velocity increases near the walls of the channel, and the trend is reversed in the middle of the channel. This situation is realistic, because the fluid velocity is no longer equal to that near the walls, and larger velocities will be noticed near the walls when the slip occurs at the walls.

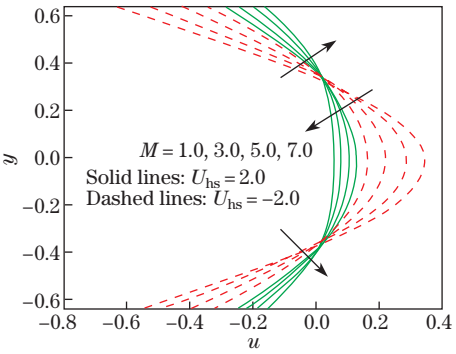

Fig. 2 Effects of M on u (color online)

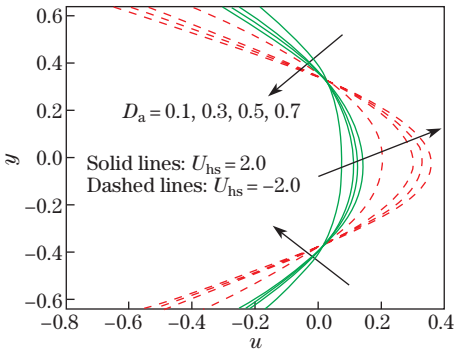

Fig. 3 Effects of D_a on u (color online)

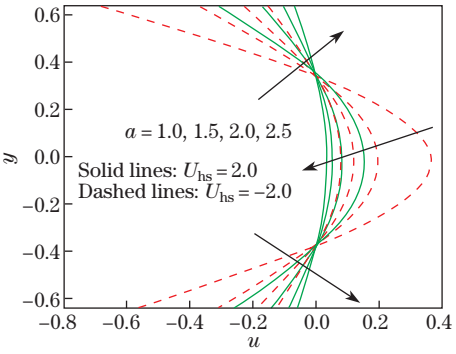

Fig. 4 Effects of a on u (color online)

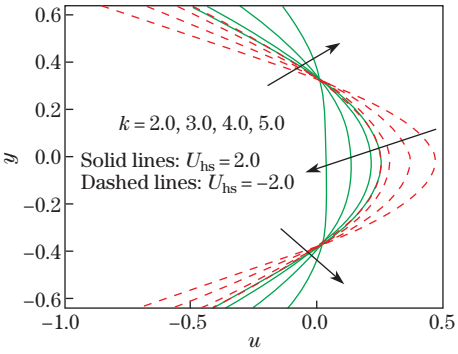

Fig. 5 Effects of k on u (color online)

Figures 7–11 show the impacts of γ, N_t, N_b, R_n, and B_h on the nanoparticle temperature distributions. Figure 7 shows that the nanoparticle temperature decreases when the value of γ increases. Figures 8–11 show the effects of N_t, N_b, R_n, and B_h on the nanoparticle temperature distributions, respectively. Note that the nanoparticle temperature increases with higher values of N_t, N_b, R_n, and B_h. The thermophoresis parameter is directly affected by the thermophoresis diffusion coefficient, which enhances the movement of nanofluids, and consequently the particles gain kinetic energy, resulting in an increase in the nanoparticle temperature of nanofluids (see Fig. 8). An increase in Brownian motion increases the random motion of the nanoparticles. This increment in random movement causes the particles to gain energy, and thus there will be an increase in the nanoparticle temperature with the increment in the Brownian motion parameter (see Fig. 9). Figure 12 illustrates the effect of N_t on the nanoparticle concentration. The thermophoresis parameter tends to enhance the nanoparticle concentration in the channel. Figure 13 shows that the concentration diminishes when the Brownian motion parameter increases.

The skin-friction coefficient distributions on the right wall of a symmetric channel for different values of D_a, M, and k are presented in Figs. 14–16. These figures show that the shear stress behavior is oscillatory, which may be due to peristalsis. With increasing values of the Darcy number, the skin friction decreases to a certain range of x, and then the skin friction

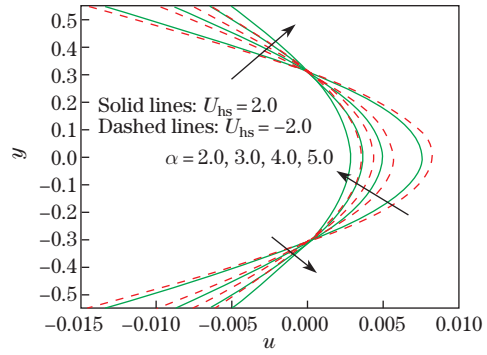

Fig. 6 Effects of α on u (color online)

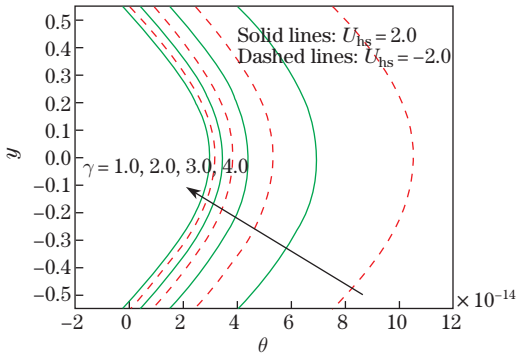

Fig. 7 Effects of γ on θ (color online)

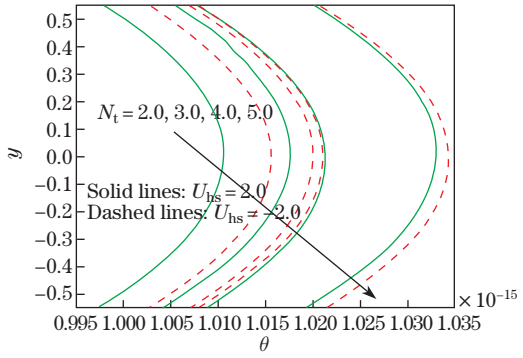

Fig. 8 Effects of N_t on θ (color online)

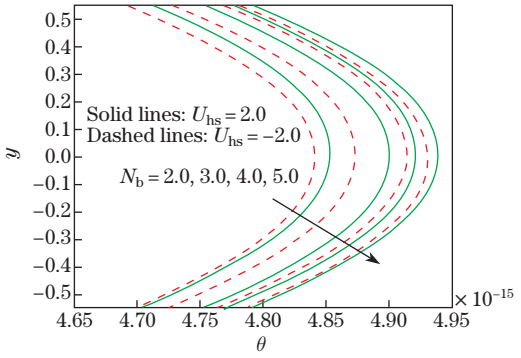

Fig. 9 Effects of N_b on θ (color online)

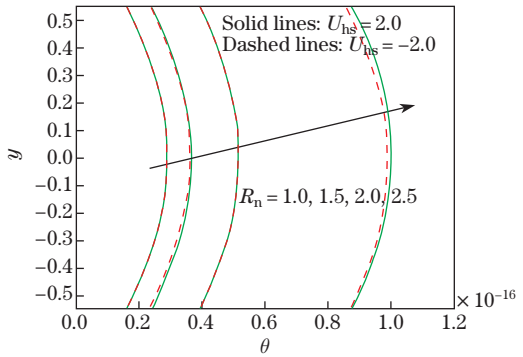

Fig. 10 Effects of R_n on θ (color online)

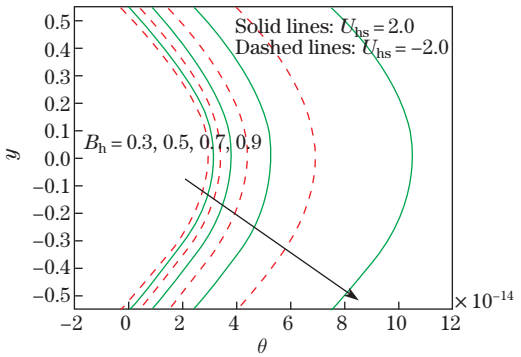

Fig. 11 Effects of B_h on θ (color online)

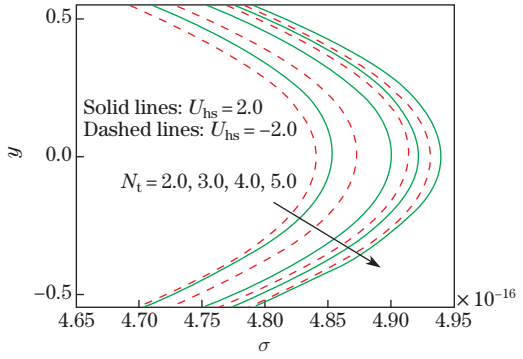

Fig. 12 Effects of N_t on σ (color online)

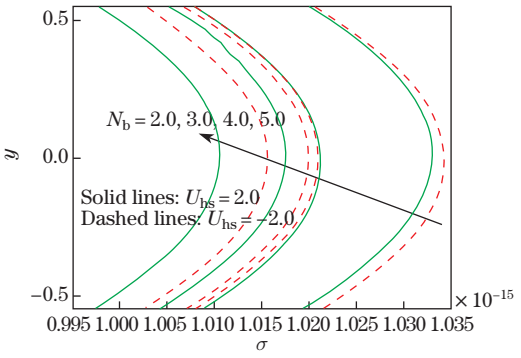

Fig. 13 Effects of N_b on σ (color online)

increases (see Fig. 14). From Figs. 15–16, the skin friction increases for a particular range of x, and then the trend is reversed with an increase in the Hartmann number and electro-osmosis parameter. Figures 17–19 depict the impacts of various parameters such as R_n, N_t, and N_b on the magnitudes of the nanoparticle heat transfer coefficient. The graphical results of the nanoparticle heat transfer coefficient are oscillatory in nature owing to the peristaltic motion of walls. Figure 17 shows that the heat transfer rate decreases for larger radiation parameters. Figure 18 shows the heat transfer coefficient for larger values of the thermophoresis parameter. Figure 19 shows that the heat transfer coefficient decreases with larger values of the Brownian motion parameter. The nanoparticle concentration coefficient Sh on the right wall of a symmetric channel for different values of N_t and N_b is presented in Figs. 20–21. These

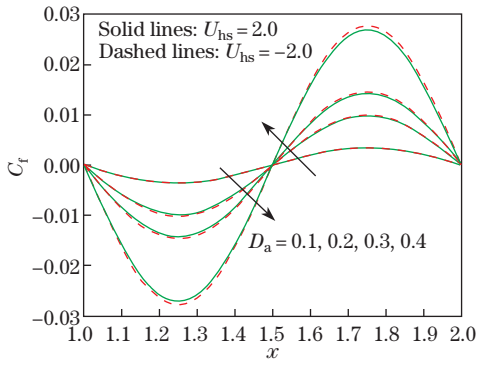

Fig. 14 Effects of D_a on C_f (color online)

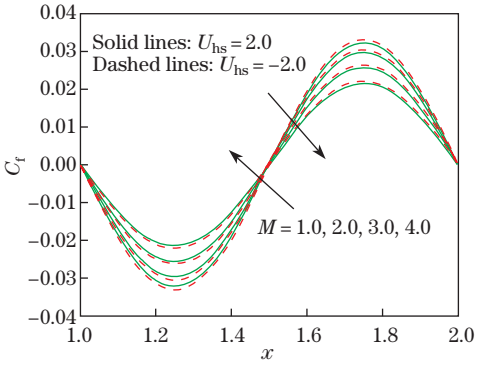

Fig. 15 Effects of M on C_f (color online)

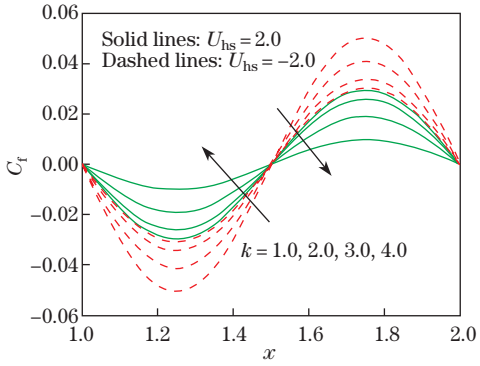

Fig. 16 Effects of k on C_f (color online)

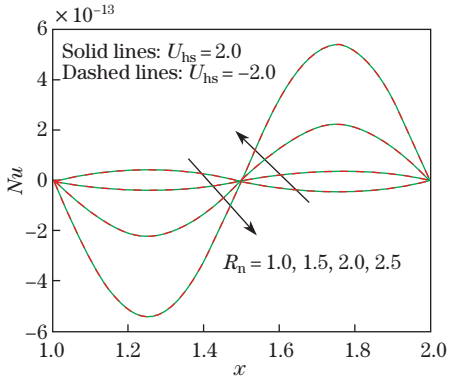

Fig. 17 Effects of R_n on Nu (color online)

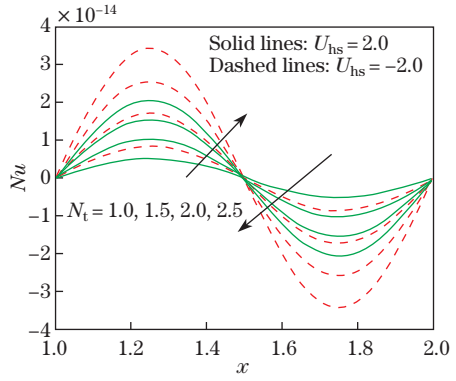

Fig. 18 Effects of N_t on Nu (color online)

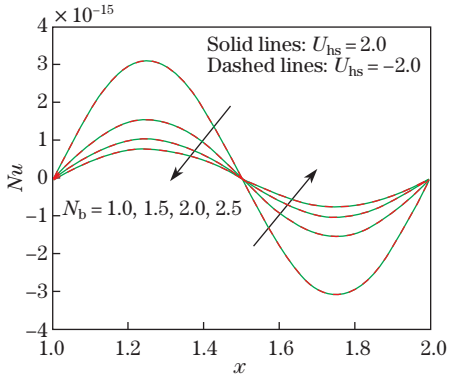

Fig. 19 Effects of N_b on Nu (color online)

figures exhibit an oscillatory behavior, which may be due to peristalsis. The absolute value of shear stress increases with increasing values of N_t whereas different behaviors are observed for N_b in Figs. 20–21. An intriguing phenomenon in the transport of fluid is trapping. It is presented through streamline sketches in Figs. 22–24. The trapped bolus is found to expand by increasing M, as shown in Figs. 22(a)–22(d). However, the size of the bolus decreases owing to the rising effects of D_a and k, as shown in Figs. 23–24.

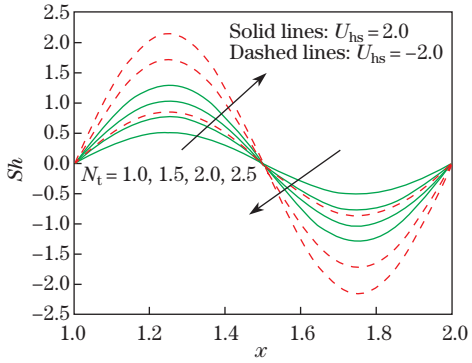

Fig. 20 Effects of N_t on Sh (color online)

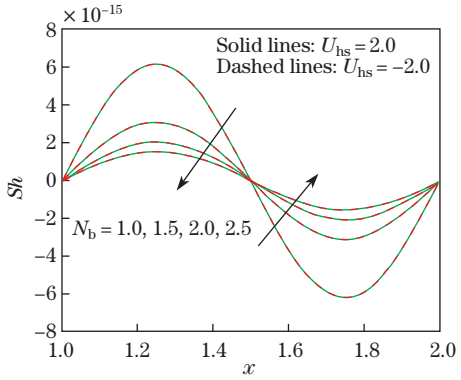

Fig. 21 Effects of N_b on Sh (color online)

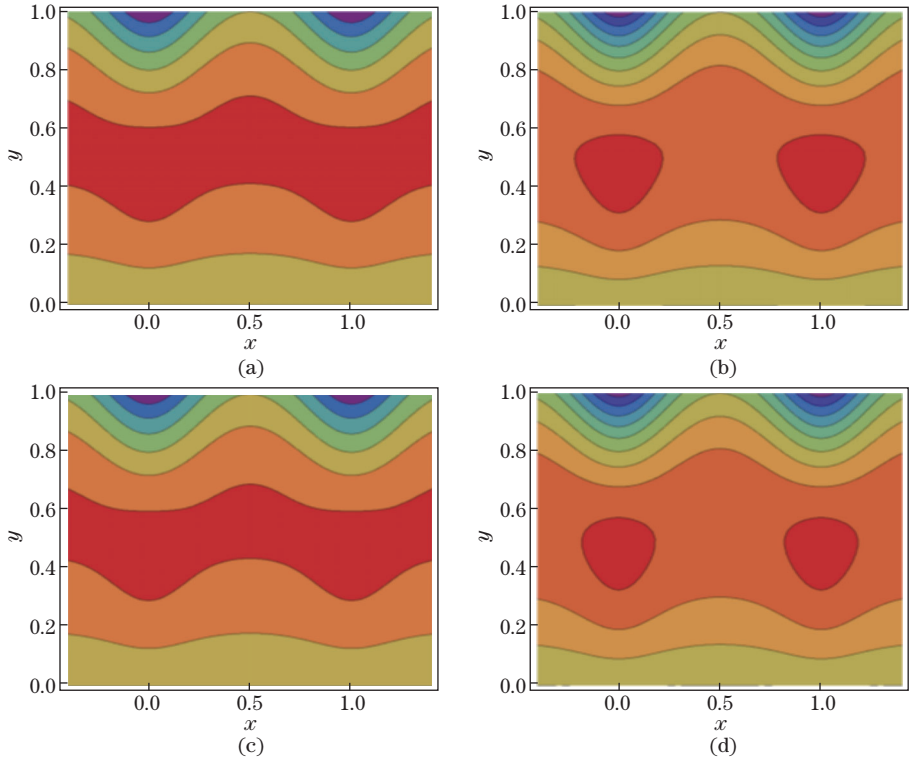

Fig. 22 Streamlines for (a) $U_{hs} = 2.0$, $M = 1.0$, (b) $U_{hs} = 2.0$, $M = 3.0$, (c) $U_{hs} = -2.0$, $M = 1.0$, and (d) $U_{hs} = -2.0$, $M = 3.0$ (color online)

4 Conclusions

A mathematical model is used to analyze the combined effects of the transverse magnetic field and the axial electrical field on two-dimensional micro-peristaltic channels with different

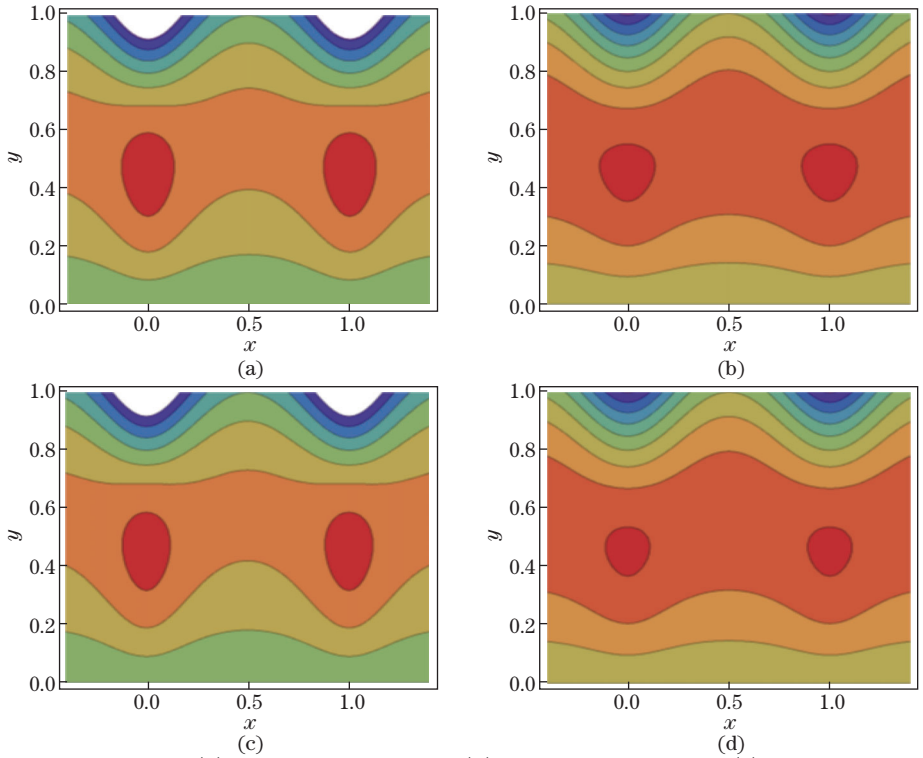

Fig. 23 Streamlines for (a) $U_{\rm hs} = 2.0$, $D_{\rm a} = 0.1$, (b) $U_{\rm hs} = 2.0$, $D_{\rm a} = 1.0$, (c) $U_{\rm hs} = -2.0$, $D_{\rm a} = 0.1$, and (d) $U_{\rm hs} = -2.0$, $D_{\rm a} = 1.0$ (color online)

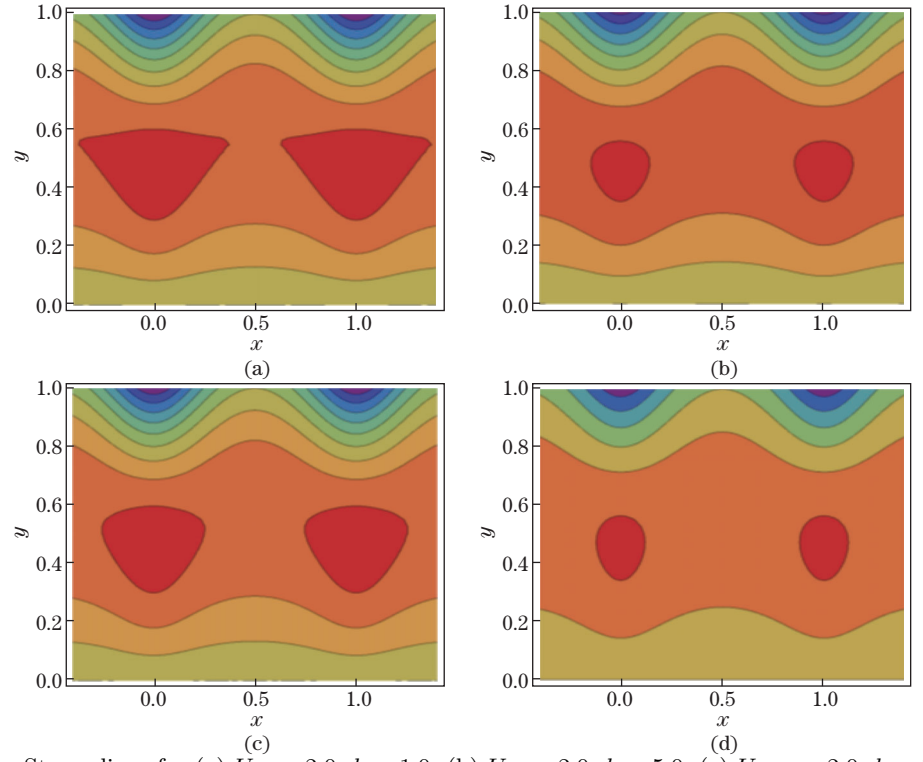

Fig. 24 Streamlines for (a) $U_{\rm hs} = 2.0$, $k = 1.0$, (b) $U_{\rm hs} = 2.0$, $k = 5.0$, (c) $U_{\rm hs} = -2.0$, $k = 1.0$, and (d) $U_{\rm hs} = -2.0$, $k = 5.0$ (color online)

peristaltic wave propagations at the left and right channel walls (complex wavy scenario) of a couple stress nanofluid. Additionally, the effects of Hall currents, porous medium, thermal radiation, heat source/sink, and slip convective boundary conditions are studied and evaluated. The governing equations are solved using a numerical procedure with the help of NDSolve MATHEMATICA under suitable boundary conditions. The key findings of this study are summarized as below.

(i) The velocity decreases for the increasing values of the Hartmann number.

(ii) An increment in the Darcy number leads to an enhancement in the velocity in the core region.

(iii) Stronger electro-osmosis yields an enhancement in the velocity.

(iv) Nanoparticle concentration increases for the thermophoresis parameter.

(v) A downfall phenomenon is observed in nanoparticle concentration for the Brownian motion parameter.

(vi) Nanoparticle heat transfer decay is recorded for a larger radiation parameter.

(vii) A larger thermophoresis parameter causes an increment in the heat transfer coefficient of nanoparticles.

(viii) The magnetic field tends to enhance the size of the bolus.

References

[1] DE LOUBENS, C., MARGIN, A., VERIN, E., DOYENNETTE, M., CRISTIA, L. T., and SOUCHON, I. A lubrication analysis of pharyngeal peristalsis: application to flavour release. *Journal of Theoretical Biology*, **267**, 300–311 (2010)

[2] BOKKA, K. K., JESUDASON, E. C., WARBURTON, D., and LUBKIN, S. R. Morphogenetic implications of peristaltic fluid-tissue dynamics in the embryonic lung. *Journal of Theoretical Biology*, **382**, 372–385 (2015)

[3] MISHRA, M. and RAO, A. R. Peristaltic transport in a channel with a porous peripheral layer: model of a flow in gastrointestinal tract. *Journal of Biomechanics*, **38**, 779–789 (2004)

[4] FRANCESCO, M., FERRUA, M. J., and SINGH, R. P. Experimental characterization of the fluid dynamics in an in-vitro system simulating the peristaltic movement of the stomach wall. *Procedia Food Science*, **1**, 1473–1478 (2011)

[5] HSU, Y. C., LI, J. H., and LE, N. B. An experimental and numerical investigation into the effects of diffuser valves in polymethylmethacrylate (PMMA) peristaltic micropumps. *Sensors and Actuators A: Physical*, **148**, 149–157 (2008)

[6] MISHRA, M., RAO, A. R., and ANGEW, Z. Peristaltic transport of a Newtonian fluid in an asymmetric channel. *Journal of Applied Mathematics and Physics*, **54**, 532–550 (2003)

[7] SRINIVAS, S. and KOTHANDAPANI, M. Peristaltic transport in an asymmetric channel with heat transfer. *International Communications in Heat and Mass Transfer*, **35**, 514–522 (2008)

[8] EBAID, A. Effects of magnetic field and wall slip conditions on the peristaltic transport of a Newtonian fluid in an asymmetric channel. *Physics Letters A*, **372**, 4493–4499 (2008)

[9] KOTHANDAPANI, M. and SRINIVAS, S. Peristaltic transport of a Jeffrey fluid under the effect of magnetic field in an asymmetric channel. *International Journal of Non-Linear Mechanics*, **43**, 915–924 (2008)

[10] SRINIVAS, S. and GAYATHRI, R. Peristaltic transport of a Newtonian fluid in a vertical asymmetric channel with heat transfer and porous medium. *Applied Mathematics and Computation*, **215**, 185–196 (2009)

[11] NADEEM, S. and AKBAR, N. S. Peristaltic flow of a Jeffrey fluid with variable viscosity in an asymmetric channel. *Zeitschrift für Naturforschung A*, **64**, 713–722 (2009)

[12] ABBASI, F. M., HAYAT, T., ALSAEDI, A., and AHMED, B. Soret and Dufour effects on peristaltic transport of MHD fluid with variable viscosity. *Applied Mathematics & Information Sciences*, **8**, 211–219 (2014)

[13] HAYAT, T., ABBASI, F. M., and AHMAD, B. Peristaltic transport of Carreau-Yasuda fluid in a curved channel with slip effects. *PLoS One*, **4**, 95070 (2014)

[14] HAYAT, T., ABBASI, F. M., AHMAD, B., and AlSAEDI, A. MHD mixed convection peristaltic flow with variable viscosity and thermal conductivity. *Sains Malaysiana*, **43**, 1583–1590 (2014)

[15] HLEW, H. S., FUNG, Y. C., and LOWENSTEIN, C. B. Peristaltic carrying and mixing of chyme in the small intestine (an analysis of a mathematical model of peristalsis of the small intestine). *Journal of Theoretical Biology*, **4**, 297–315 (1971)

[16] TRIPATHI, D. A mathematical model for the peristaltic flow of chyme movement in small intestine. *Mathematical Biosciences*, **233**, 90–97 (2011)

[17] BERTUZZI, A., SALINARI, S., MANCINELLI, R., and PESCATORI, M. Peristaltic transport of a solid bolus. *Journal of Theoretical Biology*, **16**, 459–464 (1983)

[18] MORADI, H. V., ZANDI, S., and FLORYAN, J. M. Algorithm for analysis of peristaltic annular flows. *Computers and Fluids*, **147**, 72–89 (2017)

[19] TSUI, Y. Y. A novel peristaltic micropump with low compression ratios. *International Journal for Numerical Methods in Fluids*, **69**, 1363–1376 (2012)

[20] KUMAR, B. V. R. and NAIDU, A. K. B. A numerical study of peristaltic flows. *Computers and Fluids*, **24**, 161–176 (1995)

[21] NATARAJAN, S. and MOKHTARZADEH, M. R. D. Numerical prediction of flow in a model of a (potential) soft acting peristaltic blood pump. *International Journal for Numerical Methods in Fluids*, **32**, 711–724 (2000)

[22] RADHAKRISHNAMACHARYA, G. and SRINIVASULU, C. Influence of wall properties on peristaltic transport with heat transfer. *Comptes Rendus Mechaniques*, **335**, 369–373 (2007)

[23] CHU, H. Stability of flows in a peristaltic transport. *Mechanics Research Communications*, **30**, 623–628 (2003)

[24] LIN, Q., YANG, B., XIE, J., and TAI, Y. C. Dynamic simulation of a peristaltic micropump considering coupled fluid flow and structural motion. *Journal of Michromechanics and Microengineering*, **17**, 220 (2007)

[25] LISA, J. F. Peristaltic pumping of solid particles. *Computers and Fluids*, **21**, 583–598 (1992)

[26] JAFFRIN, M. Y. Inertia and streamline curvature effects on peristaltic pumping. *International of Engineering Science*, **11**, 681–699 (1973)

[27] BERG, J. M., ANDERSON, R., ANAYA, M., LAHLOUH, B., HOLTZ, M., and DALLAS, T. A two-stage discrete peristaltic micropump. *Sensors and Actuators A: Physical*, **104**, 6–10 (2003)

[28] AFIFI, N. A. S. and GAD, N. S. Interaction of peristaltic flow with pulsatile fluid through a porous medium. *Applied Mathematics and Computation*, **142**, 167–176 (2003)

[29] PHILIP, J. and SHIMA, P. D. Thermal properties of nanofluids. *Advances in Colloid and Interface Science*, **183**, 30–45 (2012)

[30] WEN, D., LIN, G., VAFAEI, S., and ZHANG, K. Review of nanofluids for heat transfer applications. *Particuology*, **7**, 141–150 (2009)

[31] SAIDUR, R., LEONG, K. Y., and MOHAMMAD, H. A review on applications and challenges of nanofluids. *Renewable and Sustainable Energy Reviews*, **15**, 1646–1668 (2011)

[32] SKARIMI, A., FAKHROUEIAN, Z., BAHRAMIAN, A., POUR-KHIABANI, N., DARABADI, J. B., AZIN, R., and ARYA, S. Wettability alteration in carbonates using zirconium oxide nanofluids: EOR implications. *Energy Fuel*, **26**, 1028–1036 (2012)

[33] YU, W., FRANCE, D. M., CHOI, S. U. S., and ROUTBORT, J. L. Review and assessment of nanofluid technology for transportation and other applications. *Technical Report*, U. S. Department of Energy, Washington, D. C. (2007)

[34] HALEFADL, S., ESTELLE, P., and MARE, T. Heat transfer properties of aqueous carbon nanotubes nanofluids in coaxial heat exchanger under laminar regime. *Experimental Thermal and Fluid Science*, **55**, 174–180 (2014)

[35] WILLIAM, J. K. M., PONMANI, S., SAMUEL, R., NAGRANJAN, R., and SANGWAI, J. S. Effect of CuO and ZnO nanofluids in xanthan gum on thermal, electrical and high pressure rheology of water-based drilling fluids. *Journal of Petroleum Science and Engineering*, **117**, 15–27 (2014)

[36] KULKARNI, D. P., DAS, D. K., and VAJJHA, R. S. Application of nanofluids in heating buildings and reducing pollution. *Applied Energy*, **86**, 2566–2573 (2009)

[37] BUONGIORNO, J., HU, L. W., KIM, S. J., HANNINK, R., TRUONG, B. A. O., and FORREST, E. Nanofluids for enhanced economics and safety of nuclear reactors: an evaluation of the potential features, issues, and research gaps. *Nuclear Technology*, **162**, 80–91 (2008)

[38] VASSALLO, P., KUMAR, R., and D'AMICO, S. Pool boiling heat transfer experiments in silica-water nano-fluids. *International Journal of Heat and Mass Transfer*, **47**, 407–411 (2004)

[39] DEMIRBAS, M. F. Thermal energy storage and phase change materials: an overview. *Energy Sources*, *Part B*: *Economics*, *Planning*, *and Policy*, **1**, 85–95 (2006)

[40] TYAGI, H., PHELAN, P., and PRASHER, R. Predicted efficiency of a low-temperature nanofluid-based direct absorption solar collector. *Journal of Solar Energy Engineering*, **131**, 41004 (2009)

[41] HAYAT, T., ABBASI, F. M., Al-YAMI, M., and MONAQUEL, S. Slip and Joule heating effects in mixed convection peristaltic transport of nanofluid with Soret and Dufour effects. *Journal of Molecular Liquids*, **194**, 93–99 (2014)

[42] ABBASI, F. M., HAYAT, T., AHMAD, B., and CHEN, G. Q. Peristaltic motion of non-Newtonian nanofluid in an asymmetric channel. *Zeitschrift für Naturforschung*, **69a**, 451–461 (2004)

[43] SHEHZAD, S. A., ABBASI, F. M., HAYAT, T., and ALSADDI, V. MHD mixed convective peristaltic motion of nanofluid with Joule heating and thermophoresis effects. *PLoS One*, **9**(11), 111417 (2014)

[44] NOREEN, S., WAHEED, S., and HUSSANAN, A. Peristaltic motion of MHD nanofluid in an asymmetric micro-channel with Joule heating, wall flexibility and different zeta potential. *Boundary Value Problems*, **2019**, 12 (2019)

[45] HAYAT, T., FAROOQ, S., ALSAEDI, A., and AHMAD, B. Numerical analysis for radial MHD and mixed convection effects in peristalsis of non-Newtonian nanomaterial with zero mass flux conditions. *Results in Physics*, **7**, 451–458 (2017)

[46] HAYAT, T., SHAFIQUE, M., TANVEER, A., and ALSAEDI, A. Magnetohydrodynamic effects on peristaltic flow of hyperbolic tangent nanofluid with slip conditions and Joule heating in an inclined channel. *International Journal of Heat and Mass Transfer*, **102**, 54–63 (2016)

[47] SHEHZAD, S. A., ABBASI, F. M., HAYAT, T., and ALSADDI, F. MHD mixed convection peristaltic motion of nanofluid with Joule heating and thermophoresis effects. *PLoS One*, **9**, 111417 (2014)

[48] HAYAT, T., NISAR, Z., AHMAD, B., and YASMIN, H. Simultaneous effects of slip and wall properties on MHD peristaltic motion of nanofluid with Joule heating. *Journal of Magnetism and Magnetic Materials*, **395**, 48–58 (2015)

[49] RAMESH, K. and PRAKASH, J. Thermal analysis for heat transfer enhancement in electroosmosis-modulated peristaltic transport of Sutterby nanofluids in a microfluidic vessel. *Journal of Thermal Analysis and Calorimetry*, **138**, 1311–1326 (2019)

[50] RAMESH, K., KUMAR, D., and DEVAKAR, M. Electrokinetically modulated flow of couple stress magnetonanofluids in a microfluidic channel. *Heat Transfer — Asian Research*, **48**, 379–397 (2019)

[51] RAMESH, K., REDDY, M. G., and DEVAKAR, M. Biomechanical study of magnetohy drodynamic Prandtl nanofluid in a physiological vessel with thermal radiation and chemical reaction. *Proceedings of the Institution of Mechanical Engineers*, *Part N*: *Journal of Nanomaterials*: *Nanoengineering and Nanosystems*, **232**(4), 95–108 (2018)